FULL PAPER

In Situ Studies of Surface-Plasmon-Resonance-Coupling Sensor Mediated by Stimuli-Sensitive Polymer Linker

Ji-Eun Lee, Kyungwha Chung, Jumi Lee, Kwanwoo Shin, and Dong Ha Kim**

Hybrid plasmonic nanostructures comprising gold nanoparticle (AuNP) arrays separated from Au substrate through a temperature-sensitive poly(N-isopropylacrylamide) (PNIPAM) linker layer are constructed, and unique plasmonic-coupling-based surface plasmon resonance (SPR) sensing properties are investigated. The optical properties of the model system are investigated by in situ and scan-mode SPR analysis. The swelling-shrinking transitions in the polymer linker brush are studied by in situ contact-mode atomic force microscopy at two different temperatures in water. It is revealed that the thickness of the PNIPAM layer is decreased from 30 to 14 nm by increasing the temperature from 20 to 32 °C. For the first time the dependence of the coupling behavior in AuNPs is investigated with controlled density on the temperature in a quantitative manner in terms of the change in SPR signals. The device containing AuNPs with optimized AuNP density shows 3.2-times enhanced sensitivity compared with the control Au film-PNIPAM sample. The refractive index sensing performance of the Au film-PNIPAM-AuNPs is greater than that of Au film-PNIPAM by 19% when the PNIPAM chains have a collapsed conformation above lower critical solution temperature.

1. Introduction

Surface plasmon resonance (SPR) is a unique optical property observed at the interface between metal and a dielectric, with the resonant excitation of surface plasmon coupled oscillations of surface electrons, and a resultant enhanced local electromagnetic field.[1–7] Noble metal nanostructures have excellent optoelectronic properties due to the localized surface plasmon resonance (LSPR) phenomenon,[8–19] and their potential functions have been demonstrated in photovoltaics,[20] photocatalysis,[21] electronics,[22] magnetics,[23] optics,[24,25] light emission,[26–28] and sensing.[29–35]

J.-E. Lee, K. Chung, Prof. D. H. Kim
Department of Chemistry and Nano Science
Division of Molecular and Life Sciences
College of Natural Sciences
Ewha Womans University
52 Ewhayeodae-Gil
Seodaemun-Gu, Seoul 03760, South Korea
E-mail: dhkim@ewha.ac.kr
J. Lee, Prof. K. Shin
Department of Chemistry
Interdisciplinary Program of Integrated Biotechnology
Sogang University
35, Baekbeom-ro, Mapo-gu, Seoul 04107, South Korea
E-mail: kwshin@sogang.ac.kr

DOI: 10.1002/adfm.201503340

Recently, great attention has been devoted to understanding the role of surface plasmon coupling between adjacent nanoscale metal objects. Many pioneering works on the coupling behaviors have been reported based on theoretical and experimental means.[36–52] Typically, the assembly of plasmonic nanostructures can induce near-field coupling of surface plasmons, leading to the generation of hot spots that are actively exploited for surface-enhancing Raman scattering (SERS).[53–58]

As a representative and alternative approach to utilize the plasmonic properties of noble metals, Kretschmann-configuration-based SPR sensing has been widely utilized.[59–62] Notably, the use of Au nanoparticles (AuNPs) or nanorods for signal amplification in this setup has afforded significantly improved sensitivity. Several researchers have developed SPR sensor chips with AuNPs integrated to utilize the coupling between LSPR and propagating SP of the basal Au substrate.[57,63–69]

Recent strategies to develop advanced sensors with more versatile functions have been explored, among which increasing attention has been paid to the anchoring of stimuli-responsive layers on Au surfaces, which allows for switchable sensory behaviors driven by changes in external environments.[70–72] Combining stimuli-sensitive layers containing AuNPs with planar Au films has been explored to demonstrate various sensory features arising from the signal amplification and responsive nature. Several pioneering works on such responsive SPR coupling systems were recently reported utilizing pH-sensitive[73–75] or temperature-sensitive[70,76] linker molecules.

Tokareva et al. deposited a thin layer of polyglycidyl methacrylate (PGMA) onto Au film, and carboxyl group-terminated pH-responsive poly(2-vinyl pyridine) brushes (P2VP-COOH) were anchored via the reaction of the epoxy group of PGMA with the end carboxylic groups of the P2VP. Then, AuNPs were loaded onto the P2VP layer, and the pH-change-induced SPR coupling phenomenon was monitored by observing the shift of the absorption maximum.[73] In another work, a similar coupling model was constructed by loading AuNPs onto a P4VP-on-Au thin-film substrate.[75] Strong interparticle plasmon coupling induced by the formation of linear and branched AuNP chains were reported upon the change in pH in the range of 2–7 in the UV–visible absorption spectra. Kang et al. established enhanced SPR spectroscopy by placing AuNPs on superoxide dismutase (SOD) tethered to the Au film of an SPR

setup.[74] Regular switching behavior with minimum reflectivity was assessed in the SPR spectrum induced by the reversible pH-driven conformational change of SOD. However, in all of the previous reports, the AuNPs were incorporated into the backbone of the polymer chains or into the responsive layers in a random manner. Moreover, none of these works systematically investigated the effect of the areal density of the top AuNP arrays, and no concrete sensory properties of the entire SPR coupling units have been demonstrated. In order to investigate the temperature-sensitive reversible switching behavior in SPR coupling models, Gupta et al. developed a useful Au-NP-coated poly(N-isopropylacrylamide)-Au substrate model via a stepwise strategy for surface modification of Au substrates. The model involves atom transfer radical polymerization (ATRP) and Click chemistry.[76] The SPR coupling properties of the temperature-sensitive model were investigated by SERS, but a more in-depth study was not demonstrated with the entire unit incorporated into a Kretschmann-type SPR setup.

It is well known that stimuli-responsive polymers undergo reversible swelling and shrinking under external stimuli such as pH, temperature, solvent polarity, and mechanical stress. Poly(N-isopropylacrylamide) (PNIPAM) is a typical thermo-responsive polymer, and it exhibits a lower critical solution temperature (LCST) at ≈32 °C in water. The phase transition changes a PNIPAM linker brush from hydrophilic to hydrophobic, intervening in the interaction between the chains and water molecules. The PNIPAM chains interact with water molecules by hydrogen bonding below LCST, and hence remain in the swollen state. If the temperature is increased above the LCST, the chains are shrunken by the formation of intramolecular hydrogen bonding. If PNIPAM chains are coupled with AuNPs, the temperature-induced change in SPR coupling properties can be explored. Utilizing the PNIPAM-AuNP assembly as a model responsive material, we have developed an advanced SPR-coupling-based sensor chip via integration of PNIPAM onto the Au substrate in Kretschmann configuration. Importantly, we have controlled the lateral density of the tethered AuNPs onto the PNIPAM layers, and systematically investigated the coupling behavior between the LSPR of AuNPs and propagating SPR of the basal Au substrate. The overall procedure to fabricate the stimuli-sensitive SPR coupling sensor is schematically illustrated in **Scheme 1**.

A disulfide initiator was immobilized onto the surface of Au film (Au film-initiator), and surface initiated ATRP of N-isopropylacrylamide (NIPAM) was performed on Au film catalyzed by N,N,N,N,N-pentamethyldiethylenetriamine (PMDETA) and CuBr. Next, azidation and Click chemistry were performed with propargylamine to generate amine functionality at the other end of the chains. Finally, AuNPs were immobilized onto each end group of individual chains using citrate-capped AuNPs, leading to the completion of the Au film-PNIPAM-AuNP assembly. The areal density of the anchored AuNPs was controlled by varying the deposition time of PNIPAM-modified Au substrates into the AuNP colloidal solution. This reversible stretching-shrinking of the polymer chains leads to a change in SPR signals. The incorporation of AuNPs can induce the overall signal amplification, which is responsible for the significant improvement in sensitivity. We systematically evaluate the modulated sensibility of the SPR-coupling-based sensor chip fabricated, as a function of the areal density of AuNP arrays. The degree of sensitivity enhancement upon the incorporation of AuNPs into the assembly was quantitatively evaluated. Finally, the viability and value of the function for sensory applications are further demonstrated in terms of the refractive index sensing using glycerol solutions with various concentrations.

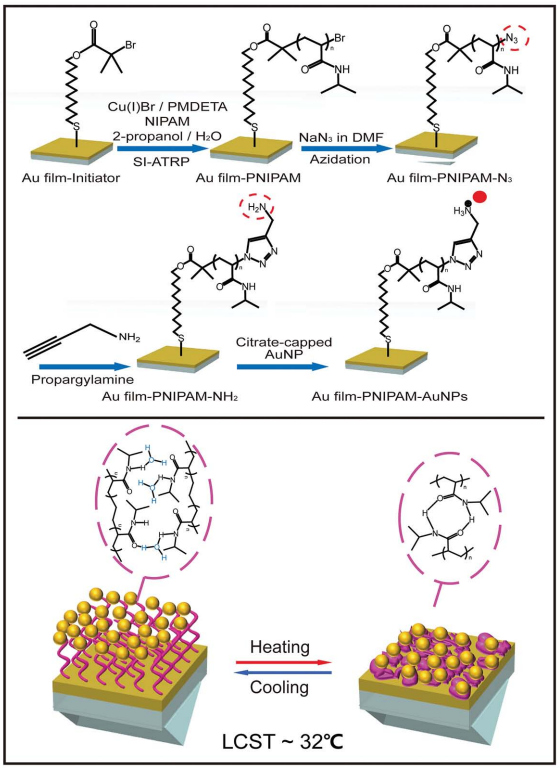

Scheme 1. Schematic diagrams for the stepwise synthetic procedure of Au film-PNIPAM-AuNP assembly (top) and for the reversible swelling-shrinking transition upon the change in temperature below and above the LCST (bottom).

2. Results and Discussion

The surface morphology of the samples for each step of the synthetic process in Scheme 1 was studied by tapping-mode atomic force microscopy (AFM). **Figure 1**A,B shows the AFM images of a bare Au film and an identical substrate after immobilization of disulfide initiator by covalent bonding, respectively. The stepwise fabrication process of the films and their thicknesses were monitored by SPR spectroscopy. The resulting Au film-initiator sample exhibits an SPR angle centered around 25.5°, with a redshift of 0.1° compared to the initial bare Au film. In general, the angular shifts of SPR curves by an increase in the areal density of Au film are quite small, and no particular deformation of SPR curves is detected, because the single-strand and alkyl chain disulfide initiator induce only a small change in the film thickness and refractive index at the interface. Figure 1C shows the smooth surface morphology of Au film-PNIPAM with top and perspective views, and the root-mean-squared (rms) roughness evaluated by the analysis of

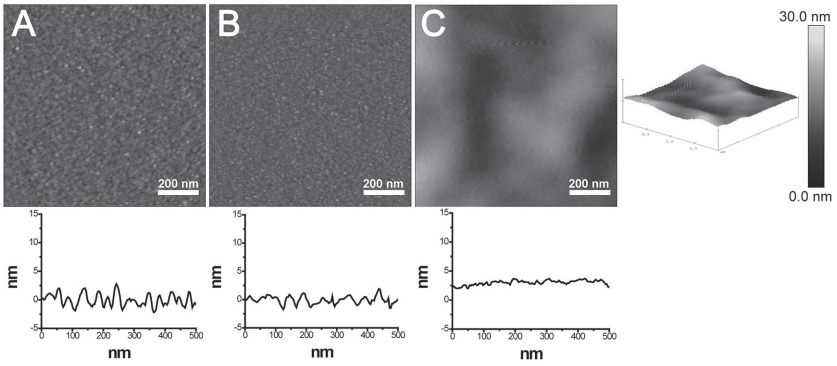

Figure 1. Height contrast AFM images of the sample surfaces. A) Bare Au film; B) Au film-initiator; C) Au film-PNIPAM (left), perspective view (right).

AFM height image was about 2.5 nm. ATR-FTIR spectrum of the PNIPAM linker brush grafted on Au film was obtained to confirm the chemical identity (**Figure 2**). Characteristic peaks of PNIPAM were observed at 1650, 1370, and 2970 cm^{-1}, which can be assigned to the C=O stretching, mixed vibration of C=H and N=H, and antisymmetric deformation of CH_3, respectively. These observed peak positions are essentially the same as those observed for pure PNIPAM.[77,78] Therefore, we concluded that PNIPAM was successfully synthesized by SI-ATRP. Gel permeation chromatography (GPC) measurements were carried out to measure the M_n of surface-grafted PNIPAM. Free standing polymers were generated by adding free initiators during the surface-initiated ATRP, and the value obtained was 22 377 $gmol^{-1}$ (see Figure S1 in the Supporting Information). The PNIPAM thickness was measured to be about 40 nm, as confirmed by the fitting result obtained using Winspall program (Table S1, Supporting Information).

Next, we discuss the results on the immobilization of AuNPs onto the amine-terminated PNIPAM layers. The diameter of the AuNPs is about 15 nm, and the LSPR band is observed at 519 nm. In order to confirm that the presence of amine functionality is crucial to accommodate the AuNPs at the chain ends, we compared the SEM images of Au film-PNIPAM-N_3 and Au film-PNIPAM-NH_2 after AuNP deposition (see Figure S3 in the Supporting Information). The amine groups of a grafted PNIPAM linker brush can be protonated and positively charged, thus allowing for the anchoring of AuNPs at the end of PNIPAM brushes via the electrostatic interaction between amine groups and citrate-capped AuNPs. Comparing the two images, it is evident that the AuNPs were immobilized onto Au film-PNIPAM-NH_2 by electrostatic interaction. **Figure 3** shows the coverage of AuNPs on the Au film-PNIPAM-NH_2 surface after immersion in the AuNP colloidal solution for different periods of time. It is clearly observed that the areal density of AuNPs increased monotonically with increasing deposition time, which is found to be responsible for the observed variation in the SPR responses.

To examine the lateral distribution of AuNPs more precisely, SEM images were analyzed using ImageJ software. The areal densities of AuNPs were calculated to be ≈2.1%, 4.8%, 11.8%, 19.0%, and 50.0% for the samples prepared with dipping times of 15 min, 30 min, 1 h, 3 h, and 24 h, respectively. It is observed that the AuNPs with different areal densities in all the samples are randomly dispersed without forming any aggregates. To confirm the formation process of the sequential assembly on the surface of the Au film, each deposition step was monitored by angle-resolved SPR measurements. **Figure 4** shows the scan-mode SPR spectra obtained from each step of the entire stepwise fabrication process. The SPR angle of the Au film-initiator was centered around 25.5°, with a redshift of 0.1° with respect to the initial bare Au film. The SPR angle after modifying the Au surface with PNIPAM was about 38.6° (Figure 4A), with a resonance angle shift of $\Delta\theta = 13.1°$ with respect to the Au film-initiator, and an increase in the width of the resonance curve. The large angular shift as well as the change in the shape of the SPR curve observed in Figure 4 can be attributed to the high and complex dielectric constant of AuNPs. As the areal density is increased, changes in the position and the magnitude of the SPR reflectivity minimum become larger, ultimately attaining a total plasmon angle shift of ≈23.2° and a reflectance increase of 37% for the Au film-PNIPAM-AuNPs (1 h)

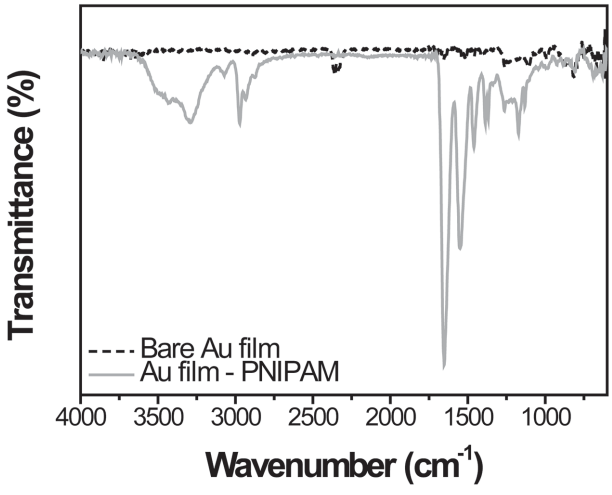

Figure 2. ATR-Fourier transformed infrared (FT-IR) spectra of bare Au film and Au film-PNIPAM synthesized by sequential SI-ATRP.

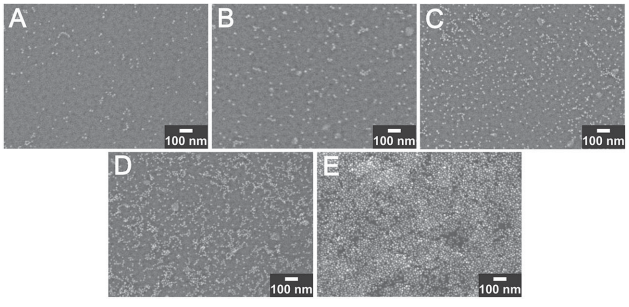

Figure 3. The SEM images of Au film-PNIPAM-AuNPs with different areal densities of the tethered AuNPs obtained by applying different immersion times: A) Au film-PNIPAM-AuNPs (15 min), B) Au film-PNIPAM-AuNPs (30 min), C) Au film-PNIPAM-AuNPs (1 h), D) Au film-PNIPAM-AuNPs (3 h), E) Au film-PNIPAM-AuNPs (24 h).

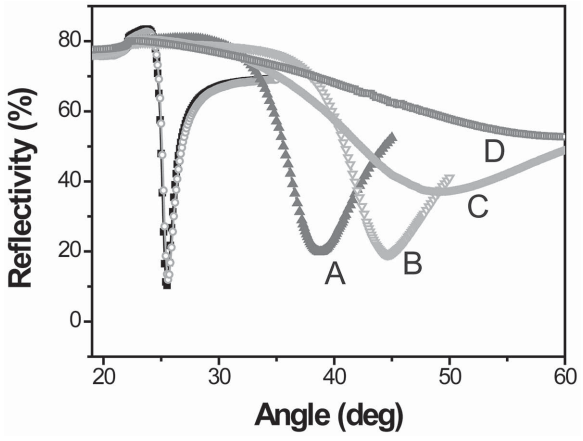

Figure 4. The scan-mode SPR spectra of bare Au film (■), Au film-initiator (○), A) Au film-PNIPAM, B) Au film-PNIPAM-AuNPs (15 min), C) Au film-PNIPAM-AuNPs (1 h), D) Au film-PNIPAM-AuNPs (3 h). All the spectra were recorded in an air environment.

(Figure 4C). It is noted that the plasmon scattering induced by the significant increase in the areal density contributes to damping (Figure 4D). Conclusively, the use of AuNPs for signal amplification resulted in significantly improved sensitivity, as evidenced by the substantial shift in SPR angles.

Next, in situ contact-mode AFM measurement was performed to determine the thickness of PNIPAM at two different temperatures in water and the results are summarized in **Figure 5**. It was observed that the conformation of the polymer chains was reversibly changed depending on the temperature. It was revealed that the thickness of the PNIPAM layer was decreased from 30 to 14 nm by increasing the temperature from 20 to 32 °C. Additionally, we investigated the surface morphology of the samples at each temperature by in situ tapping-mode AFM. In the AFM image, the collapse of the polymer chains led to an increase in the surface roughness, as shown in Figure S2C (Supporting Information). The surface roughness of the Au film-PNIPAM was observed to increase from 1.11 to 1.49 nm by changing the temperature from 20 to 32 °C (see Figure S2 in the Supporting Information).

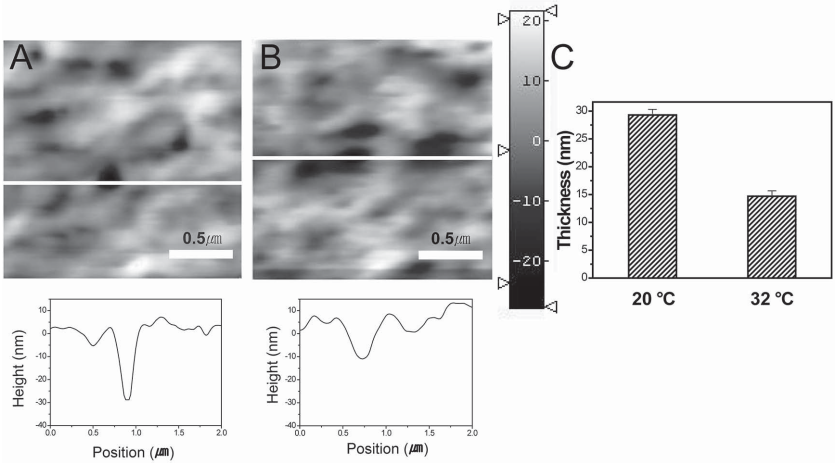

Figure 5. In situ contact mode images AFM of Au film-PNIPAM at A) 20 °C; B) 32 °C in water environment; C) average thickness plat of Au film-PNIPAM.

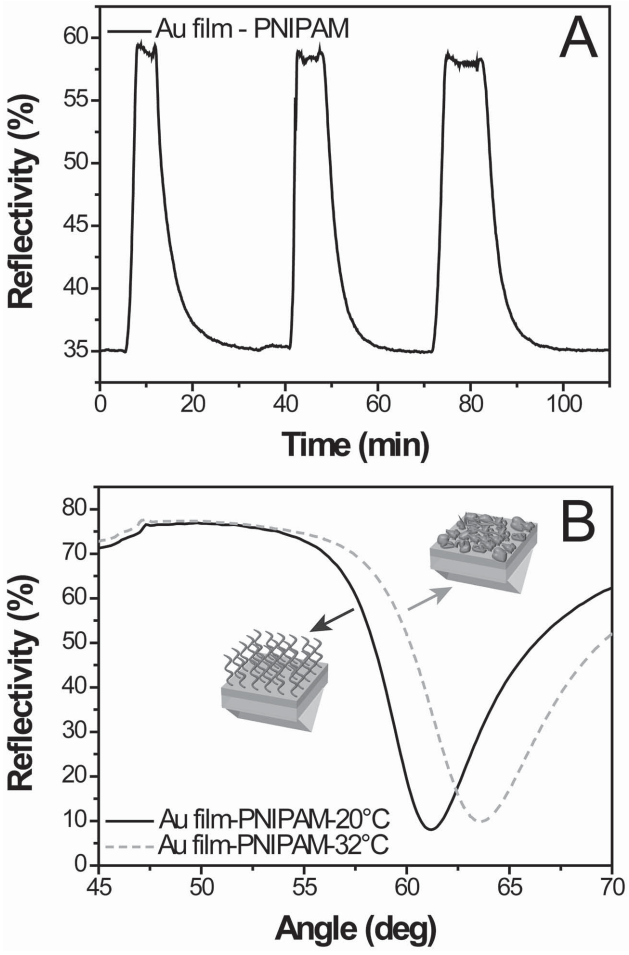

Figure 6. A) In situ kinetic-mode SPR spectrum and B) the static scan-mode SPR curves for the reversible change in the swelling-shrinking transition process at two different temperatures obtained from the Au film-PNIPAM.

Thus, we investigate the response of the SPR signal of the developed models upon the change in temperature, regarding the conformational transition of the PNIPAM chains. The sensory properties of the Au film-PNIPAM system without tethered AuNPs are discussed first using in situ kinetic- and scan-mode SPR spectroscopy, as shown in **Figure 6**A,B, respectively. It is well known that the PNIPAM chains interact with water molecules via hydrogen bonding below LCST, and hence remain in a swollen state. If the temperature is increased above the LCST, PNIPAM chains form intramolecular hydrogen bonding and collapse. As shown in Figure 6A, the time-dependent reflectance change was monitored in a water environment at a fixed angle by adjusting the temperature above and below the LCST repeatedly. Upon heating the system, the reflectivity increases quickly as a result of the conformational transition of the polymer linker brush

from swelling to shrinking states. It is clearly observed that the thermoinduced shrinking-swelling transition of the polymer linker brush is completely reversible. In the scan-mode SPR spectra, the collapse of the polymer chains led to a redshift in the SPR angle, as shown in Figure 6B. The SPR angle of the Au film-PNIPAM was observed to shift from 61.6° to 64.0° ($\Delta\theta$ = 2.4°) by changing the temperature from 20 to 32 °C. These results are correlated with the conformational change of the PNIPAM at 20 and 32 °C. The change in the thickness of PNIPAM linker brush induced the change in refractive index of PNIPAM linker brush at 20 and 32 °C. The refractive index at two different temperatures was determined to be 1.33 and 1.35 in water at 20 and 32 °C, respectively.[79]

We further investigate the response of the SPR signal of the Au film-PNIPAM-AuNP systems with different areal densities of AuNPs upon change in the temperature. **Figure 7** shows the scan-mode SPR spectra of a series of Au film-PNIPAM-AuNP systems. It is observed that the SPR angle shows redshift behavior with $\Delta\theta \approx 3.1°$, 7.5°, and 2.1° for the samples prepared with 15 min, 1 h, and 3 h dipping in AuNP colloidal solution, respectively. Notably, it was found that the shift in the SPR angle for the sample prepared with 24 h dipping was negligibly small (the scan-mode SPR profile is not shown). From these results, a few critical conclusions can be made: (i) $\Delta\theta$ increases with increasing areal density at an early stage; (ii) with further increase in the areal density, the relative degree of the shift becomes diminished (Figure 7B vs Figure 7C); (iii) once the areal density reaches a certain critical value, no noticeable shift in the SPR angle is observed. Thus, it is concluded that an optimum areal density exists to induce maximum $\Delta\theta$ resulting from the plasmonic coupling between the Au nanocluster arrays and the underlying Au film.

The reversible change in the reflectivity and SPR angle induced by repeated thermo-control cycles is summarized **Figure 8**. For the Au film-PNIPAM-AuNP sample exhibiting the maximum $\Delta\theta$ value, it is evident that the thermo-induced reversible shift of the SPR angles is quite regular, in accordance with the thermo-induced reversible shrinking-swelling transition (Figure 8A). Upon the shrinking of the PNIPAM linker brushes, the reflectivity increased from 26.4% to 45.8% (ΔR = 19.4%), and the SPR angle increased from 64.2° to 71.8° ($\Delta\theta$ = 7.6°). The overall sensitivity of the Au film-PNIPAM and Au film-PNIPAM-AuNP systems toward the change in the temperature in the form of swelling-shrinking transition is compared in Figure 8B. One can clearly see that the Au film-PNIPAM-AuNP sample shows markedly enhanced sensitivity ($\Delta\theta$ = 7.6°) that is 3.2 times greater than that of the Au film-PNIPAM ($\Delta\theta$ = 2.4°) at 32 °C. Conclusively, it was demonstrated that the presence of AuNPs in the responsive assembly leads to significantly enhanced response due to the coupling between localized and propagating surface plasmons.

In order to demonstrate the viable function of the unique SPR coupling sensor chip developed in this study, we investigate the plasmonic-coupling-based sensing activity of an Au film-PNIPAM-AuNP sample in terms of refractive index sensing. To this end, we prepared a series of glycerol solutions with various concentrations, and compared the refractive index unit (RIU) using Au film-PNIPAM and the Au film-PNIPAM-AuNPs (1 h) as model systems. The refractive index (n_a) of

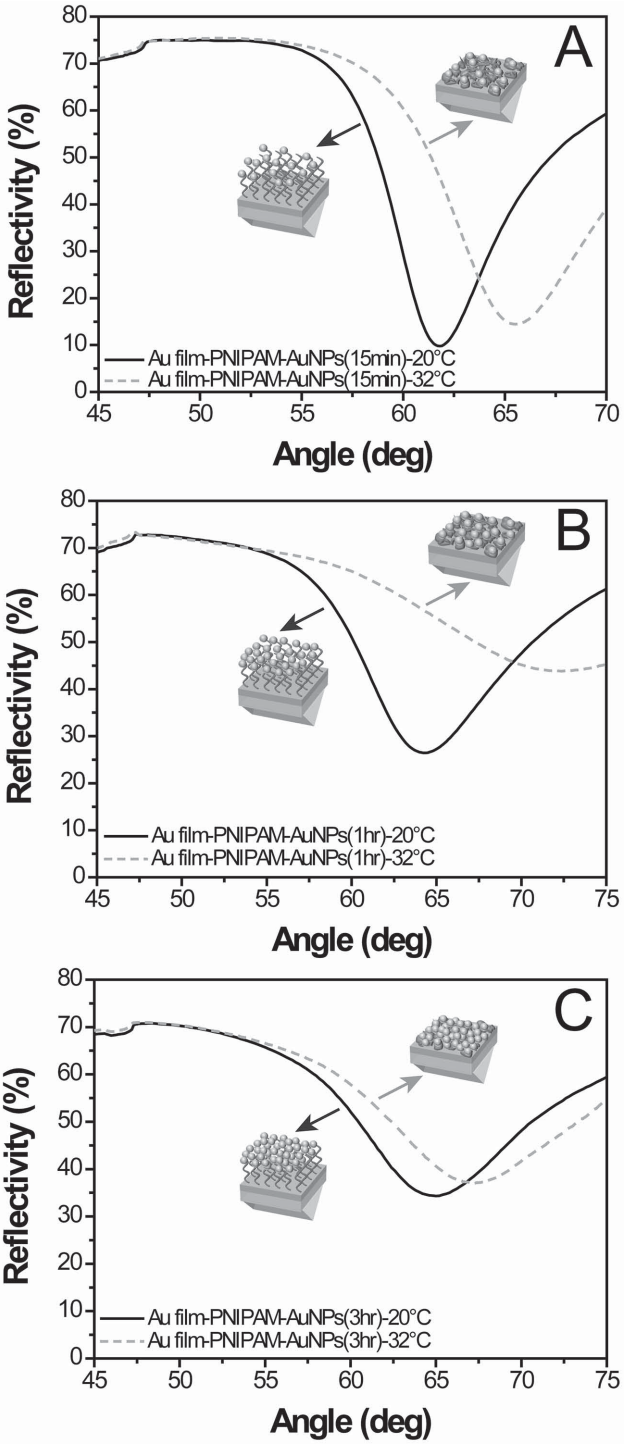

Figure 7. The static scan-mode SPR curves of Au film-PNIPAM-AuNPs with different areal densities of AuNPs obtained by immersing the Au film-PNIPAM into AuNP colloid solution for different periods of time. A) Au film-PNIPAM-AuNPs (15 min), B) Au film-PNIPAM-AuNPs (1 h), C) Au film-PNIPAM-AuNPs (3 h). All the spectra were recorded in a water environment.

glycerol solutions of 0%, 10%, 20%, and 30% concentrations correspond to 1.330, 1.345, 1.357, and 1.373, respectively. In order to check if the thermo-responsive and swelling properties

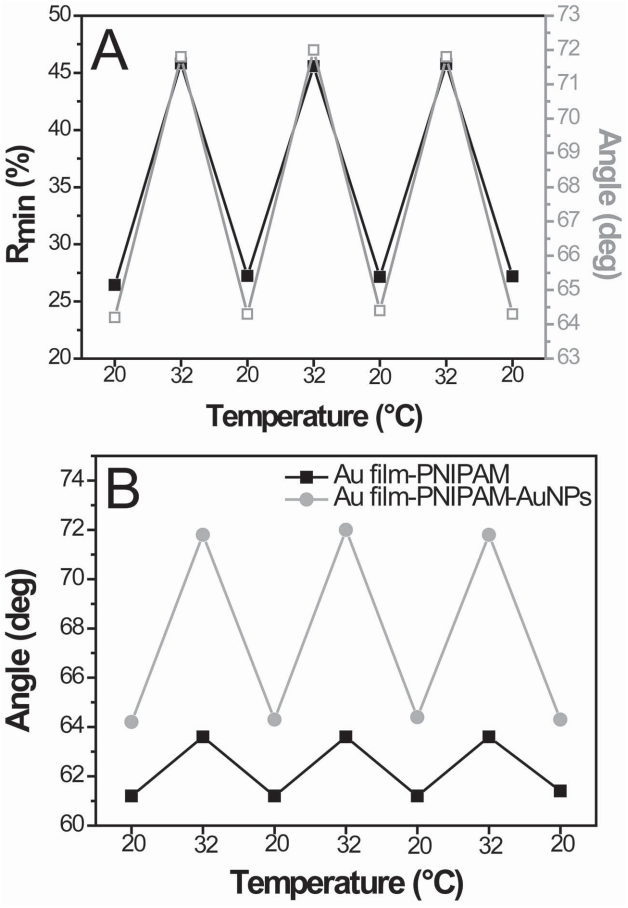

Figure 8. A) Reversible thermo-responsive changes in the reflectivity of kinetic mode and SPR angle of scan mode for the Au film-PNIPAM-AuNPs obtained by immersing Au film-PNIPAM in AuNP colloid solution for 1 h. B) Reversible changes in the reflectivity minimum of the SPR angle monitored for the Au film-PNIPAM and Au film-PNIPAM-AuNPs obtained from a 1 h dipping process.

of the PNIPAM layer in water are similar at different glycerol concentrations, we monitored the change in PNIPAM thickness as a function of glycerol concentration at 20 and 32 °C (see Figure S4 in the Supporting Information). It was found that the thickness was affected by the glycerol concentration at 20 °C, presumably because the glycerol molecules might penetrate into the PNIPAM brush layer in its extended conformation. In contrast, the thickness of the PNIPAM brush barely changed at 32 °C. Based on these observations, we limited the discussion about the sensing property of the current responsive models under 32 °C. The static scan-mode SPR curves obtained from Au film-PNIPAM and Au film-PNIPAM-AuNPs in different glycerol concentrations at 32 °C are shown in **Figure 9**A,B, respectively. It is observed that the resonance angle shifted to higher angle with increasing the glycerol concentration for both samples. Based on the SPR sensor diagram with angular modulation, the sensitivity of the devices can be evaluated by comparing the angular sensitivity parameter (denoted as S), i.e., the change in the resonant angle with respect to the variation in the refractive index of analyte, according to Equation (1)

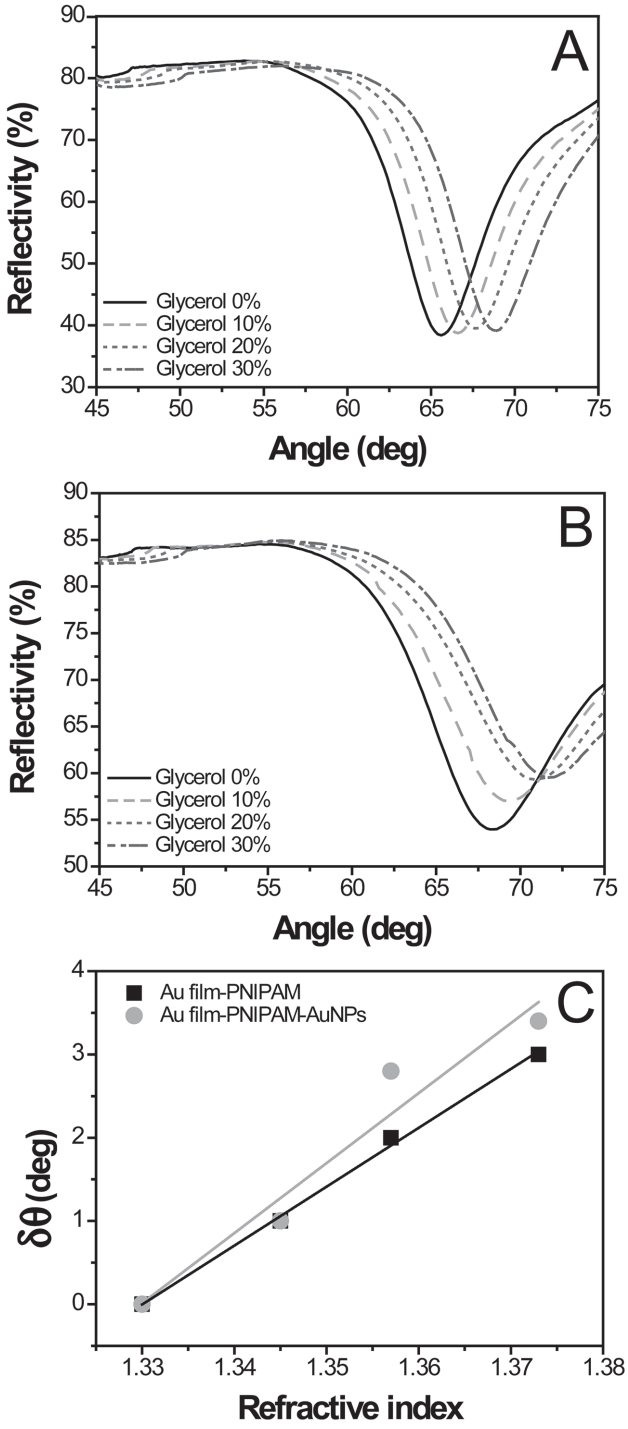

Figure 9. The static scan-mode SPR curves obtained from A) Au film-PNIPAM and B) Au film-PNIPAM-AuNPs in different glycerol concentrations at 32 °C. C) The plots for the dependence of SPR angular shift on the glycerol concentration obtained from Au film-PNIPAM and Au film-PNIPAM-AuNPs at 32 °C. Linear regression of these data produces best-fit functions of $y = 70.7x$ ($R^2 = 0.9959$) for Au film-PNIPAM at 32 °C and $y = 84.1x$ ($R^2 = 0.9204$) for Au film-PNIPAM-AuNPs (1 h) at 32 °C, where y is the shift of the SPR angles, and x is the glycerol concentration of 0%, 10%, 20% and 30%, corresponding to an index of refraction of 1.330, 1.345, 1.357 and 1.373, respectively.

$$S = \delta\theta / \delta n_a \quad (1)$$

The S parameters calculated for the Au film-PNIPAM and Au film-PNIPAM-AuNP (1 h) systems are summarized in Figure 9C. The SPR angular shift increases linearly as the glycerol concentration is increased for all the sensor chips. These results imply that the dependence of the coupled SPR field originating from the AuNP cluster arrays at 32 °C by a specific distance away from a SPR-active surface on the polymer conformational change is more complex than the simple exponential decrease of the plasmon electric field originating from a planar Au film. Comparing the S values, it is concluded that the sensor chip based on Au film-PNIPAM-AuNPs (S = 84.1° RIU^{-1}) showed higher sensitivity than Au film-PNIPAM (S = 70.7° RIU^{-1}) system. The Au film-PNIPAM-AuNPs sample showed markedly enhanced sensitivity by up to 19.0% than that of the Au film-PNIPAM under the condition explored in this study.

3. Conclusion

We have developed a unique plasmonic-coupling-based sensing device comprising AuNPs separated from the Au substrate in a Kretschmann-configuration SPR spectrometer through a thermo-responsive PNIPAM linker layer. PNIPAM was first polymerized onto the surface of Au films through a SI-ATRP process. Then, we used Click chemistry to functionalize the end group of the tethered PNIPAM chains, to which AuNPs were anchored. The optical properties of the stimuli-responsive devices fabricated were investigated by both kinetic- and scan-mode SPR analysis. The thickness change of PNIPAM layers upon the temperature change was monitored via in situ contact-mode AFM. Upon increasing the temperature from 20 to 32 °C, it was revealed that the thickness of the PNIPAM layer was decreased from 30 to 14 nm for the Au film-PNIPAM system. We investigated for the first time the dependence of the plasmonic coupling behavior of sensor chips having different AuNP areal densities on the temperature in a quantitative manner in terms of the SPR band shift. We found that a specific Au-NP-containing SPR sensor device with optimized AuNP density showed 3.2 times enhanced sensitivity compared with the control Au film-PNIPAM sample. We also demonstrated that the Au film-PNIPAM-AuNP system showed enhanced sensitivity toward refractive index sensing by 19%, higher than that of Au film-PNIPAM when the PNIPAM chains have a collapsed conformation above LCST. Thus, advanced stimuli-sensitive SPR-coupling-based sensory devices with quantified performance are suggested, which can find enormous potential in practical bio-sensing and biotechnology applications.

4. Experimental Section

Materials: 11-Mercapto-1-undecanol, 2-bromo-2-methylpropionyl bromide, CuBr, N-isopropylacrylamide (NIPAM, 97%), $HAuCl_4$, sodium citrate, sodium azide, 2-propargylamine, copper(II) sulfate ($CuSO_4$), L-ascorbic acid sodium salt, and PMDETA were purchased from Sigma-Aldrich. The disulfide initiator $[S–(CH_2)_{11}OCOC-(CH_3)_2Br]_2$ for SI-ATRP was synthesized from 11-mercapto-1-undecanol and 2-bromo-2-methylpropionyl bromide through a modified procedure according to a procedure reported elsewhere.[80]

Preparation of Au film: 50-nm-thick Au film was deposited on glass substrate (LaSFN9, JMC Glass Inc., Korea) with a 2-nm Cr layer to promote adhesion, using vacuum evaporation (SHE-6D-350D, Samhan Vacuum Inc., Korea).

Synthesis of AuNPs: 150 mL of distilled water and 1.5 mL of $HAuCl_4$ solution (25.4×10^{-3} M) were added into a 250 mL round-bottom flask, and the solution was brought to boil on a hot plate with vigorous stirring. Then, 0.9 mL of sodium citrate solution (170×10^{-3} M) was added rapidly, and the solution was boiled for another 20 min under stirring. The color of the solution eventually turned to deep red. The concentration of AuNPs used was 3.1×10^{-9} M.

Preparation of SI-ATRP Initiator on Au Film: The disulfide initiator was immobilized on the surface of Au film. Bare Au film was immersed into a disulfide initiator solution (6 µL, 1.0×10^{-3} M) in ethanol (10 mL) for 24 h. Then, the Au film-initiator substrate was collected, and washed with ethanol and deionized water. The bromo-terminated Au film is referred to herein as Au film-initiator.

SI-ATRP Process of PNIPAM: Polymerization of NIPAM on an Au surface was performed in a mixed solvent in ambient conditions. In detail, a round-bottom Schlenk flask was filled with CuBr (12.5 mg, 0.085 mmol), NIPAM (0.905 g, 8 mmol), and Au film-initiator substrate degassed by three freeze–pump–thaw cycles in N_2 atmosphere. A degassed mixture of PMDETA (0.04 mL, 0.48 mmol) dissolved in H_2O (15.2 mL), methanol (2 mL) and a certain amount of free initiator (10 µL) were injected into the flask through a syringe. The reaction was performed for 1 h at room temperature and terminated by opening the system to air. The Au film-PNIPAM substrate was rinsed by washing with water.

Immobilization of AuNPs on Au film–PNIPAM substrate: The conversion of bromo-end groups of PNIPAM to azide functions was implemented by reacting the Au film–PNIPAM substrate in sodium azide (65 mg, 1 mmol) and DMF (10 mL) for 1 h at room temperature (Scheme 1). The azide-terminated Au film is referred to as Au film–PNIPAM–N_3. The Au film–PNIPAM–N_3 substrate, copper(II) sulfate (0.24 mg, 0.15 mmol), and L-ascorbic acid sodium salt (6.6 mg, 0.0375 mg) were added into a Schlenk flask equipped with a magnetic stirring bar. The system was degassed by three freeze–pump–thaw cycles in N_2 atmosphere. In the frozen state, water (12.5 mL), ethanol (12.5 mL), and 2-propargylamine (8.2 mg, 0.15 mmol) were added under N_2 atmosphere for 24 h at 25 °C. The resulting amine-terminated Au film is referred to as Au film–PNIPAM–NH_2. Finally, the immobilization of AuNPs onto the amine groups was accomplished by immersing the Au film–PNIPAM–NH_2 sample in the AuNP solution for different amounts of time (15 min, 30 min, 1 h, 3 h, 24 h), followed by thorough rinsing with water.

SPR Measurements: SPR measurements were performed using a Kretschmann configuration setup. The sample and the detector were mounted onto a two-axis θ–2θ coaxial goniometer, which enabled precise tuning of the SPR angle of the incident light and the detector. The Au thin film was illuminated through a prism with a linearly p-polarized, frequency-modulated laser (HeNe, λ = 632.8 nm, power = 10 mW). The intensity of the reflected light was recorded by a photodiode detector connected to a lock-in amplifier. All the SPR measurements were conducted with in situ and scan modes using a closed-flow cell. The flow cell size was $\pi \times 4^2 \times 7$ mm^3, and a peristaltic pump was used for liquid handling. The flow cell was filled with deionized water obtained from a Milli-Q system with a resistivity of 18.2 MΩ cm. With an electronically controlled, water-cooled resistive heater, the temperature of the flow cell was set at a fixed temperature.

Instruments: Transmission electron microscope (TEM) measurements were carried out using a JEOL JSM2100-F microscope operated at 100 kV. UV–vis absorption spectra were recorded on a Varian Technologies Cary 5000. SPR measurements were carried out using a Resonant Technologies GmbH / RT2005 SPR spectrometer. AFM studies on the surface morphologies of the nanostructured thin films on Au film on glass slides were performed with a Digital Instruments Dimension

3100 scanning force microscope in tapping mode and a surface imaging systems Picostation in contact mode. The morphologies of the nanostructures were investigated with a scanning electron microscopy (SEM; JEOL JSM6700-F). Fourier transform infrared (FT-IR) spectra were recorded on a Bruker Vertex70.

Supporting Information

Supporting Information is available from the Wiley Online Library or from the author.

Acknowledgements

This work was supported by National Research Foundation of Korea Grant funded by the Korean Government (2014R1A2A1A09005656). K. Shin and J. Lee acknowledge the Mid-career Researcher Program (2011-0017539) through National Research Foundation funded by the Korean Government.

Received: August 10, 2015
Published online: October 9, 2015

[1] G. V. Hartland, G. Schatz, *J. Phys. Chem. C* **2011**, *115*, 15121.
[2] T. W. Odom, G. C. Schatz, *Chem. Rev.* **2011**, *111*, 3667.
[3] J. H. Hafner, P. Nordlander, P. S. Weiss, *ACS Nano* **2011**, *5*, 4245.
[4] Y. Xia, N. J. Halas, *MRS Bull.* **2005**, *30*, 338.
[5] J. N. Anker, W. P. Hall, O. Lyandres, N. C. Shah, J. Zhao, R. P. Van Duyne, *Nat. Mater.* **2008**, *7*, 442.
[6] W. A. Murray, W. L. Barnes, *Adv. Mater.* **2007**, *19*, 3771.
[7] W. L. Barnes, A. Dereux, T. W. Ebbesen, *Nature* **2003**, *424*, 824.
[8] K. A. Willets, R. P. Van Duyne, *Annu. Rev. Phys. Chem.* **2007**, *58*, 267.
[9] E. Hutter, J. H. Fendler, *Adv. Mater.* **2004**, *16*, 1685.
[10] A. Moores, F. Goettmann, *New J. Chem.* **2006**, *30*, 1121.
[11] C. J. Murphy, T. K. San, A. M. Gole, C. J. Orendorff, J. X. Gao, L. Gou, S. E. Hunyadi, T. Li, *J. Phys. Chem. B* **2005**, *109*, 13857.
[12] C. Noguez, *J. Phys. Chem. C* **2007**, *111*, 3806.
[13] K. L. Kelly, E. Coronado, L. L. Zhao, G. C. Schatz, *J. Phys. Chem. B* **2003**, *107*, 668.
[14] S. Eustis, M. A. El-Sayed, *Chem. Soc. Rev.* **2006**, *35*, 209.
[15] R. Sardar, A. M. Funston, P. Mulvaney, R. W. Murray, *Langmuir* **2009**, *25*, 13840.
[16] A. M. Schwartzberg, J. Z. Zhang, *J. Phys. Chem. C* **2008**, *112*, 10323.
[17] W. B. Zhao, J. Park, A.-M. Caminade, S.-J. Jeong, Y. H. Jang, S. O. Kim, J.-P. Majoral, J. Cho, D. H. Kim, *J. Mater. Chem.* **2009**, *19*, 2006.
[18] J. Y. Lee, J. Lee, Y. J. Jang, J. Lee, Y. H. Jang, S. T. Kochuveedu, S. S. Lee, D. H. Kim, *Soft Matter* **2011**, *7*, 57.
[19] J. Y. Lee, J. Lee, Y. J. Jang, J. Lee, Y. H. Jang, S. T. Kochuveedu, C. Park, D. H. Kim, *Chem. Commun.* **2011**, *47*, 1782.
[20] Y. H. Jang, Y. J. Jang, S. T. Kochuveedu, M. Byun, Z. Lin, D. H. Kim, *Nanoscale* **2014**, *6*, 1823.
[21] S. T. Kochuveedu, D.-P. Kim, D. H. Kim, *J. Phys. Chem. C* **2012**, *116*, 2500.
[22] M. C. Daniel, D. Astruc, *Chem. Rev.* **2004**, *104*, 293.
[23] S. D. Soelberg, R. C. Stevens, A. P. Limaye, C. E. Furlong, *Anal. Chem.* **2009**, *81*, 2357.
[24] S. M. Borisov, O. S. Wolfbeis, *Chem. Rev.* **2008**, *108*, 423.
[25] J. Chen, F. Saeki, J. Benjamin, H. Cang, M. J. Cobb, Z. Y. Li, L. Au, H. Zhang, M. B. Kimmey, X. Li, *Nano Lett.* **2005**, *5*, 473.
[26] S. T. Kochuveedu, T. Son, Y. Lee, M. Lee, D. Kim, D. H. Kim, *Sci. Rep.* **2014**, *4*, 4735.
[27] S. T. Kochuveedu, J. H. Oh, Y. R. Do, D. H. Kim, *Chem. Eur. J.* **2012**, *18*, 7467.
[28] S. T. Kochuveedu, Y. H. Jang, D. H. Kim, *Chem. Soc. Rev.* **2013**, *42*, 8467.
[29] F. Yu, S. J. Tian, D. F. Yao, W. Knoll, *Anal. Chem.* **2004**, *76*, 3530.
[30] X. Lou, C. Wang, L. He, *Biomacromolecules* **2007**, *8*, 1385.
[31] N. Thanh, A. Vernhet, Z. Rosenzweig, *Springer Ser. Chem. Sens. Biosens.* **2005**, *3*, 261.
[32] K. Chung, J. Lee, J.-E. Lee, J. Y. Lee, S. Moon, K. H. A. Lau, D. Kim, D. H. Kim, *Sens. Actuators, B* **2013**, *176*, 1074.
[33] K. Chung, A. Rani, J.-E. Lee, J. E. Kim, Y. Kim, H. Yang, S. O. Kim, D. Kim, D. H. Kim, *ACS Appl. Mater. Interfaces* **2015**, *7*, 144.
[34] J.-E. Lee, K. Chung, Y. H. Jang, Y. J. Jang, S. T. Kochuveedu, D. Li, D. H. Kim, *Anal. Chem.* **2012**, *84*, 6494.
[35] D. X. Li, J. F. Zhang, Y. H. Jang, Y. J. Jang, D. H. Kim, J. S. Kim, *Small* **2012**, *8*, 1442.
[36] S. K. Ghosh, T. Pal, *Chem. Rev.* **2007**, *107*, 4797.
[37] L. M. Liz-Marzán, *Langmuir* **2006**, *22*, 32.
[38] J. M. Romo-Herrera, R. A. Alvarez-Puebla, L. M. Liz-Marzán, *Nanoscale* **2011**, *3*, 1304.
[39] L. V. Brown, H. Sobhani, J. B. Lassiter, P. Nordlander, N. J. Halas, *ACS Nano* **2010**, *4*, 819.
[40] L. S. Slaughter, Y. Wu, B. A. Willingham, P. Nordlander, S. Link, *ACS Nano* **2010**, *4*, 4657.
[41] C. Pecharromán, *Phys. Chem. Chem. Phys.* **2009**, *11*, 5922.
[42] S. S. Aćimović, M. P. Kreuzer, M. U. González, R. Quidant, *ACS Nano* **2009**, *3*, 1231.
[43] P. K. Jain, W. Huang, M. A. El-Sayed, *Nano Lett.* **2007**, *7*, 2080.
[44] P. Pramod, K. G. Thomas, *Adv. Mater.* **2008**, *20*, 4300.
[45] C. L. Haynes, A. D. McFarland, L. L. Zhao, R. P. Van Duyne, G. C. Schatz, L. Gunnarsson, J. Prikulis, B. Kasemo, M. Käll, *J. Phys. Chem. B* **2003**, *107*, 7337.
[46] V. V. Agrawal, N. Varghese, G. Kulkarni, C. Rao, *Langmuir* **2008**, *24*, 2494.
[47] J. Cho, F. Caruso, *Chem. Mater.* **2005**, *17*, 4547.
[48] B. M. Reinhard, M. Siu, H. Agarwal, A. P. Alivisatos, J. Liphardt, *Nano Lett.* **2005**, *5*, 2246.
[49] Q. H. Wei, K. H. Su, S. Durant, X. Zhang, *Nano Lett.* **2004**, *4*, 1067.
[50] Y. Yang, S. Matsubara, M. Nogami, J. Shi, W. Huang, *Nanotechnology* **2006**, *17*, 2821.
[51] W. Rechberger, A. Hohenau, A. Leitner, J. Krenn, B. Lamprecht, F. Aussenegg, *Opt. Commun.* **2003**, *220*, 137.
[52] M. Hentschel, D. Dregely, R. Vogelgesang, H. Giessen, N. Liu, *ACS Nano* **2011**, *5*, 2042.
[53] S. Nie, S. R. Emory, *Science* **1997**, *275*, 1102.
[54] S. S. R. Dasary, A. K. Singh, D. Senapati, H. Yu, P. C. Ray, *J. Am. Chem. Soc.* **2009**, *131*, 13806.
[55] Y. Fang, N. H. Seong, D. D. Dlott, *Science* **2008**, *321*, 388.
[56] J. P. Camden, J. A. Dieringer, Y. Wang, D. J. Masiello, L. D. Marks, G. C. Schatz, R. P. Van Duyne, *J. Am. Chem. Soc.* **2008**, *130*, 12616.
[57] L. A. Lyon, D. J. Peña, M. J. Natan, *J. Phys. Chem. B* **1999**, *103*, 5826.
[58] Y. S. Shon, H. Y. Choi, M. S. Guerrero, C. Kwon, *Plasmonics* **2009**, *4*, 95.
[59] J. Homola, *Surface Plasmon Resonance Based Sensors,* Vol *4*, Springer, Berlin–Heidelberg–New York **2006**.
[60] J. Homola, S. S. Yee, G. Gauglitz, *Sens. Actuators, B* **1999**, *54*, 3.
[61] W. Knoll, *Annu. Rev. Phys. Chem.* **1998**, *49*, 569.
[62] A. Abbas, M. J. Linman, Q. Cheng, *Biosens. Bioelectron.* **2011**, *26*, 1815.
[63] E. E. Bedford, J. Spadavecchia, C. M. Pradier, F. X. Gu, *Macromol. Biosci.* **2012**, *12*, 724.
[64] X. Hong, E. A. H. Hall, *Analyst* **2012**, *137*, 4712.
[65] D. E. Mustafa, T. Yang, Z. Xuan, S. Chen, H. Tu, A. Zhang, *Plasmonics* **2010**, *5*, 221.
[66] S. Gao, N. Koshizaki, H. Tokuhisa, E. Koyama, T. Sasaki, J. K. Kim, J. Ryu, D. S. Kim, Y. Shimizu, *Adv. Funct. Mater.* **2009**, *20*, 78.

[67] G. Pelossof, R. Tel-Vered, X. Q. Liu, I. Willner, *Chem. Eur. J.* **2011**, *17*, 8904.
[68] L. He, M. D. Musick, S. R. Nicewarner, F. G. Salinas, S. J. Benkovic, M. J. Natan, C. D. Keating, *J. Am. Chem. Soc.* **2000**, *122*, 9071.
[69] W. C. Law, K. T. Yong, A. Baev, P. N. Prasad, *ACS Nano* **2011**, *5*, 4858.
[70] S. Gupta, M. Agrawal, P. Uhlmann, F. Simon, M. Stamm, *Chem. Mater.* **2010**, *22*, 504.
[71] D. Li, Y. Cui, K. Wang, Q. He, X. Yan, J. Li, *Adv. Funct. Mater.* **2007**, *17*, 3134.
[72] J. Song, L. Cheng, A. Liu, J. Yin, M. Kuang, H. Duan, *J. Am. Chem. Soc.* **2011**, *133*, 10760.
[73] I. Tokareva, S. Minko, J. H. Fendler, E. Hutter, *J. Am. Chem. Soc.* **2004**, *126*, 15950.
[74] T. Kang, S. Hong, I. Choi, J. J. Sung, Y. Kim, J. S. Hahn, J. Yi, *J. Am. Chem. Soc.* **2006**, *128*, 12870.
[75] S. Z. Nergiz, S. Singamaneni, *ACS Appl. Mater. Interfaces* **2011**, *3*, 945.
[76] H. Gehan, L. Fillaud, M. Chehimi, J. Aubard, A. Hohenau, N. Felidj, C. Mangeney, *ACS Nano* **2010**, *4*, 6491.
[77] Y. Maeda, T. Higuchi, I. Ikeda, *Langmuir* **2000**, *16*, 7503.
[78] F. Meersman, J. Wang, Y. Wu, K. Heremans, *Macromolecules* **2005**, *38*, 8923.
[79] G. K. Joshi, K. A. Smith, M. A. Johnson, R. Sardar, *J. Phys. Chem. C* **2013**, *117*, 26228.
[80] R. R. Shah, D. Merreceyes, M. Husemann, I. Rees, N. L. Abbott, C. J. Hawker, J. L. Hedrick, *Macromolecules* **2000**, *33*, 597.